Surface heterogeneity effects on regional-scale fluxes in stable boundary layers: an LES study

Fernando Porté-Agel (email: fporte@umn.edu), Rob Stoll and Efi Foufoula-Georgiou
St. Anthony Falls Laboratory, Department of Civil Engineering, University of Minnesota (website: http://efd.safl.umn.edu)

Introduction

The ability to parameterize turbulent fluxes over heterogeneous terrain is dependent upon our understanding of the complex, non-linear interactions between land-surface characteristics and atmospheric boundary layer (ABL) dynamics. Under stable ABL conditions, the effect of stratification on local characteristic turbulence length scales further complicates this interaction. In this research, we use large-eddy simulation (LES), with recently developed tuning-free dynamic subgrid-scale models, to study the effect of heterogeneous surface temperature distributions on areally-averaged turbulent fluxes. The simulation setup is based on the GABLS LES intercomparison case (Beare et al., 2006) with an expanded domain. The surface heterogeneity consists of simple one-dimensional patches with different temperatures. Simulations are performed with changing patch sizes and also temperature differences between patches. Results indicate that within the surface layer both traditional and local Monin-Obukhov similarity theories fail to fully represent the average turbulent fluxes of heat and momentum. The error increases with increasing patch size and also with increasing temperature difference between patches. Above the blending height, which depends on the patch size, the turbulent fluxes follow local similarity. These results are expected to help improve parameterizations used in large-scale weather and climate models. Future research will also quantify the effect of the degree of organization of remotely sensed surface properties on the boundary layer fluxes using data from the NASA CLPX experiment.

Filtered LES equations

• Momentum:

$$\frac{\partial \tilde{u}_i}{\partial t} + \frac{\partial(\tilde{u}_i\tilde{u}_j)}{\partial x_j} = -\frac{\partial \tilde{p}}{\partial x_i} - \frac{\partial \tau_{ij}}{\partial x_j} + \delta_{i3} g \frac{(\tilde{\theta} - \langle\tilde{\theta}\rangle)}{\theta_0} + f_c \epsilon_{ij3}\tilde{u}_j + F_i$$

• Scalar concentration:

$$\frac{\partial \tilde{\theta}}{\partial t} + \tilde{u}_i \frac{\partial \tilde{\theta}}{\partial x_i} = -\frac{\partial q_j}{\partial x_j}$$

where (~) denotes filtering at the scale Δ and the subgrid scale (SGS) stress τ_{ij} and SGS flux q_i are given by,

$$\tau_{ij} = \widetilde{u_i u_j} - \tilde{u}_i\tilde{u}_j \quad \text{and} \quad q_i = \widetilde{u_i\theta} - \tilde{u}_i\tilde{\theta}$$

Scale-dependent Lagrangian dynamic SGS model

• Base Models:

Eddy viscosity $\tau_{ij} - \frac{1}{3}\delta_{ij}\tau_{kk} = -2(\Delta C_s)^2 |\tilde{S}|\tilde{S}_{ij}$

Eddy diffusion $q_i = -\Delta^2 C_s^2 Pr_{sgs}^{-1} |\tilde{S}| \frac{\partial \tilde{\theta}}{\partial x_i}$

where: ⟶ $\tilde{S}_{ij} = \frac{1}{2}\left(\frac{\partial \tilde{u}_i}{\partial x_j} + \frac{\partial \tilde{u}_j}{\partial x_i}\right)$ and $|\tilde{S}| = 2\left(\tilde{S}_{ij}\tilde{S}_{ij}\right)^{1/2}$

• Model coefficients: specification of C_S and $C_S^2 Pr_{sgs}^{-1}$:

- **Model coefficients** need to account for the change in characteristic length scale of the turbulence associated with local flow conditions.

- Scale dependent Lagrangian dynamic models are used to compute the model coefficients C_s and $C_s^2 Pr_{sgs}^{-1}$ (**Stoll and Porté-Agel, 2006**).

- The simulations are **tuning-free** since coefficients are computed at every time step and position in the flow based on the dynamics of the resolved scales.

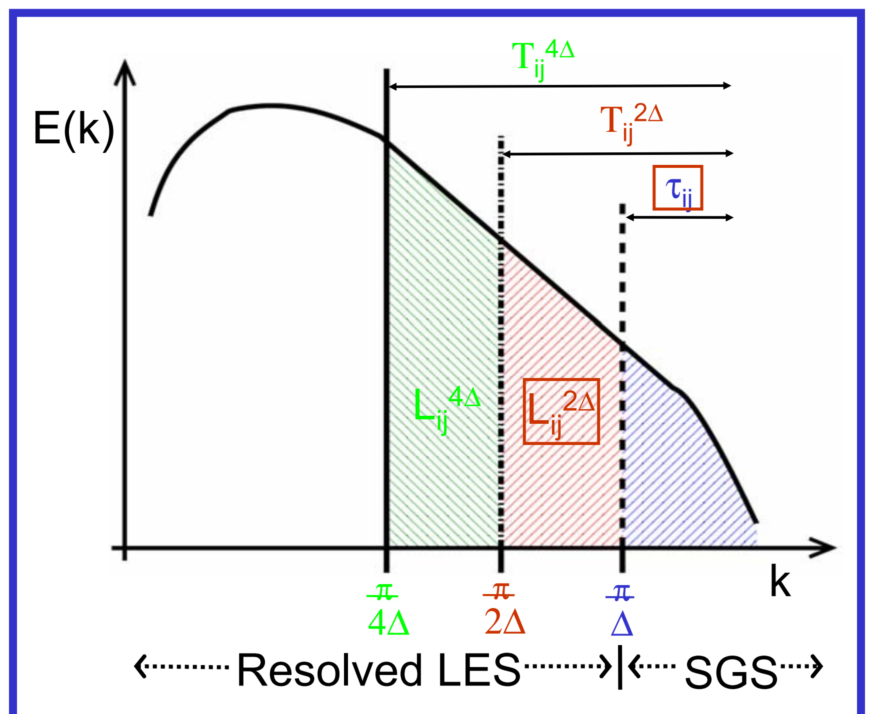

Figure 1: Schematic of the scales used in the dynamic determination of the model coefficients C_s and $C_s^2 Pr_{sgs}^{-1}$.

• Dynamic model for C_S :

- By applying the base model to compute the sub-grid fluxes at different scales (see Figure 1), and minimizing the error in the estimation of 'resolved' fluxes, we obtain:

$$C_s^2 = \frac{\langle L_{ij}M_{ij}\rangle}{\langle M_{ij}M_{ij}\rangle} \quad \text{where} \quad \begin{cases} L_{ij} = \overline{\tilde{u}_i\tilde{u}_j} - \bar{\tilde{u}}_i\bar{\tilde{u}}_j = T_{ij} - \bar{\tau}_{ij} \\ M_{ij} = 2\Delta^2\left(\overline{|\tilde{S}|\tilde{S}_{ij}} - 4\frac{C_S^2(2\Delta)}{C_S^2(\Delta)}|\bar{\tilde{S}}|\bar{\tilde{S}}_{ij}\right) \end{cases}$$

• Lagrangian averaging:

- Enforce the dynamic model backwards along fluid pathlines (Meneveau et al., 1996).

$$\langle A(\boldsymbol{x},t)\rangle = \int_{-\infty}^{t} A(\boldsymbol{z}(t'),t')T^{-1}e^{-(t-t')/T}dt'$$

- ⟨⟩ represents averaging along fluid pathlines (Figure 2) over time T at position **x**.

- previous events are weighted exponentially as we move backward along fluid particle trajectories (Figure 2).

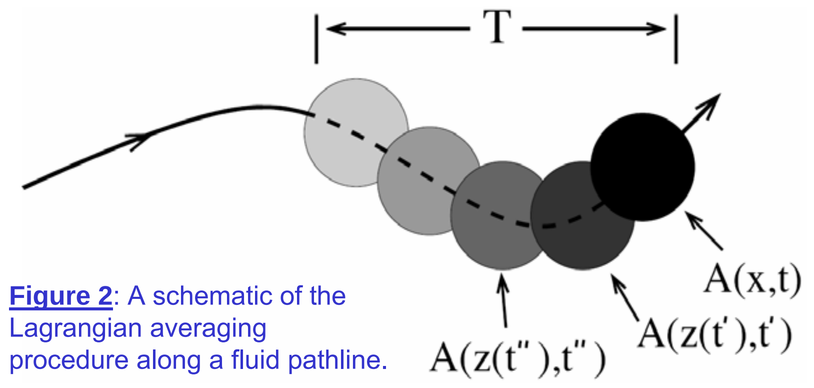

Figure 2: A schematic of the Lagrangian averaging procedure along a fluid pathline.

Homogeneous SBL case:

- Based on GABLS LES case (Beare et al. 2006)
- Domain size: **H = 400 m; Lx = Ly = 800 m**
- Resolution: $N_x \times N_y \times N_z$ = 128 x 128 x 128
- Geostrophic wind U_{geo} = 8 m/s
- Coriolis f_c = 1.39 x 10^{-4} s^{-1} (73° N)
- Surface cooling rate = 0.25 K/hr
- Surface roughness z_o = 0.1 m
- **12 hr** simulation (averages over hours 11-12)

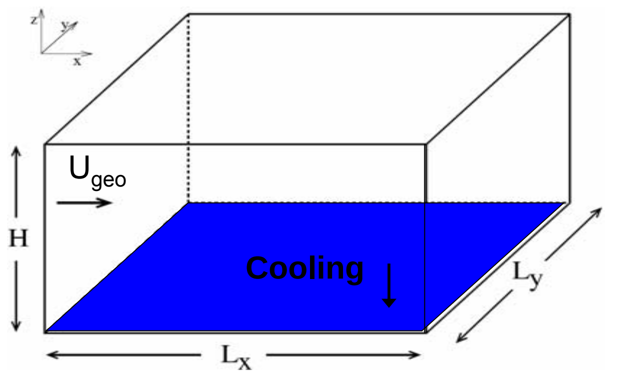

Figure 3: Schematic of the LES domain used in the homogeneous SBL cases.

case	δ (m)	u_* (m/s)	θ_* (K)	L (m)
128^3 lag	179	0.258	-0.00139	126
96^3 lag	179	0.261	-0.00139	129
64^3 lag	180	0.261	-0.00141	127
128^3 loc	185	0.262	-0.00143	126

Table 1: Mean boundary layer characteristics for the 3 homogeneous test cases with the scale-dependent Lagrangian dynamic model (Stoll and Porté-Agel, 2006) with 128^3 (128^3 lag), 96^3 (96^3 lag) and 64^3 (64^3 lag) grid points and for the local scale-dependent dynamic model of Basu and Porté-Agel (2006) with 128^3 (128^3 loc) grid points.

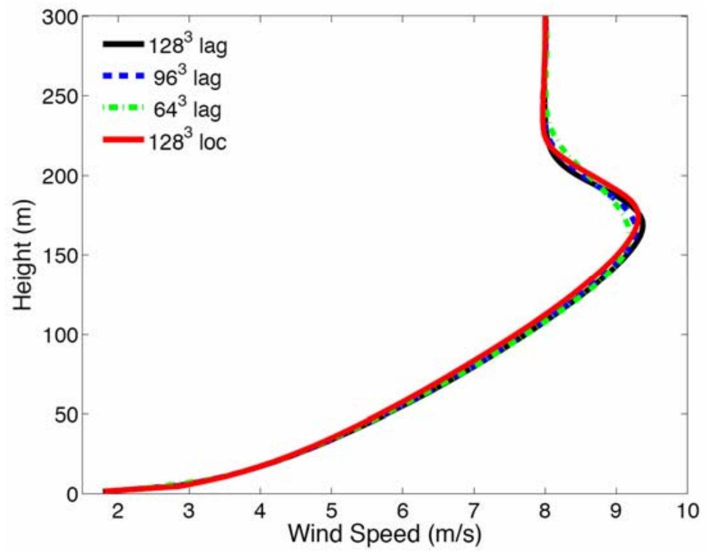

Figure 4: Mean wind speed profile averaged over the last one hour of the simulation for homogeneous stable boundary layer simulations at different resolutions. Legend abbreviations are the same as used in Table 1.

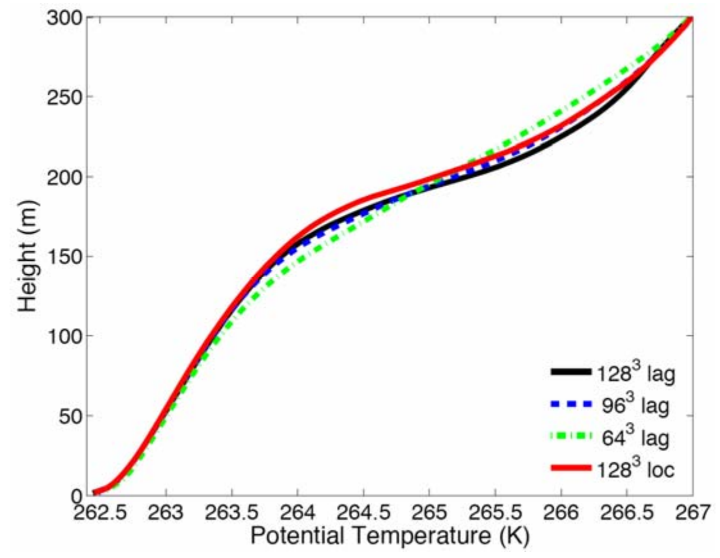

Figure 5: Mean potential temperature averaged over the last one hour of the simulation for homogeneous stable boundary layer simulations at different resolutions. Legend abbreviations are the same as used in Table 1.

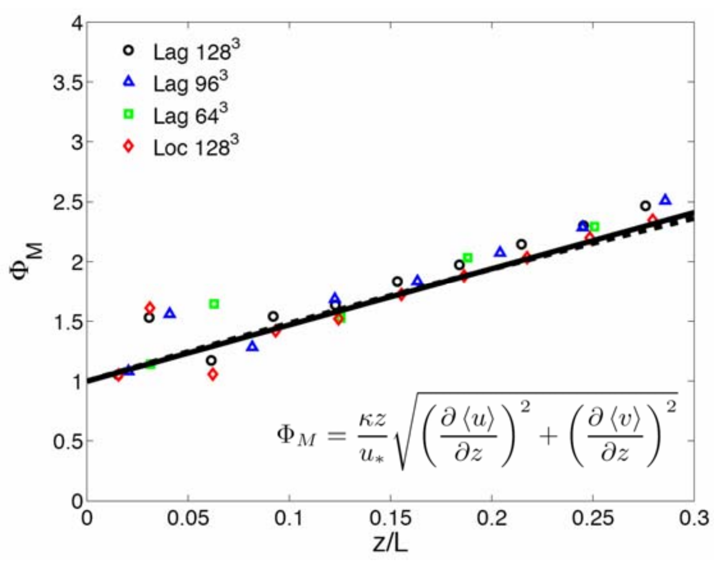

Figure 6: Non-dimensional velocity gradient as a function of z/L in the lowest 50 m of the domain. The solid line and dashed line correspond to the formulations proposed by Businger et al. (1971) and Beljaars and Holtslag (1991), respectively.

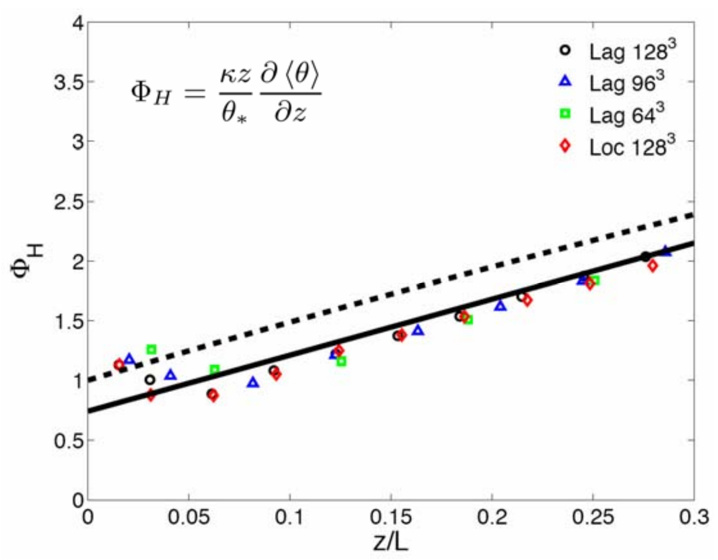

Figure 7: Non-dimensional potential temperature gradient as a function of z/L in the lowest 50 m of the domain. The solid line and the dashed line correspond to the formulations proposed by Businger et al. (1971) and Beljaars and Holtslag (1991), respectively.

Heterogeneous SBL cases:

-Surface temperature transitions-

- **8 hours heterogeneous cooling**
  - **-2 different temp jumps:**
    - **- 3 K**
    - **- 6 K**
  - **- 3 different patch sizes:**
    - **- 400 m**
    - **- 200 m**
    - **- 100 m**
- **4 hours homogeneous cooling at 0.25 K/hr**

case	δ (m)	u_* (m/s)	θ_* (K)	L (m)
Hom	179	0.258	-0.00139	126
Het3-400	186	0.261	-0.00116	152
Het3-200	185	0.262	-0.00120	148
Het3-100	184	0.263	-0.00121	148
Het6-400	207	0.270	-0.00071	273
Het6-200	202	0.271	-0.00080	240
Het6-100	200	0.272	-0.00086	225

Table 2: Mean boundary layer characteristics for the different surface types characterized by the jump (in K) and the patch length (in m): homogeneous (Hom); 3 K, 400 m (Het3-400); 3 K, 200 m (Het3-200); 3 K, 100 m (Het3-100); 6 K, 400 m (Het6-400); 6 K, 200 m (Het6-200); 6 K, 100 m (Het6-100).

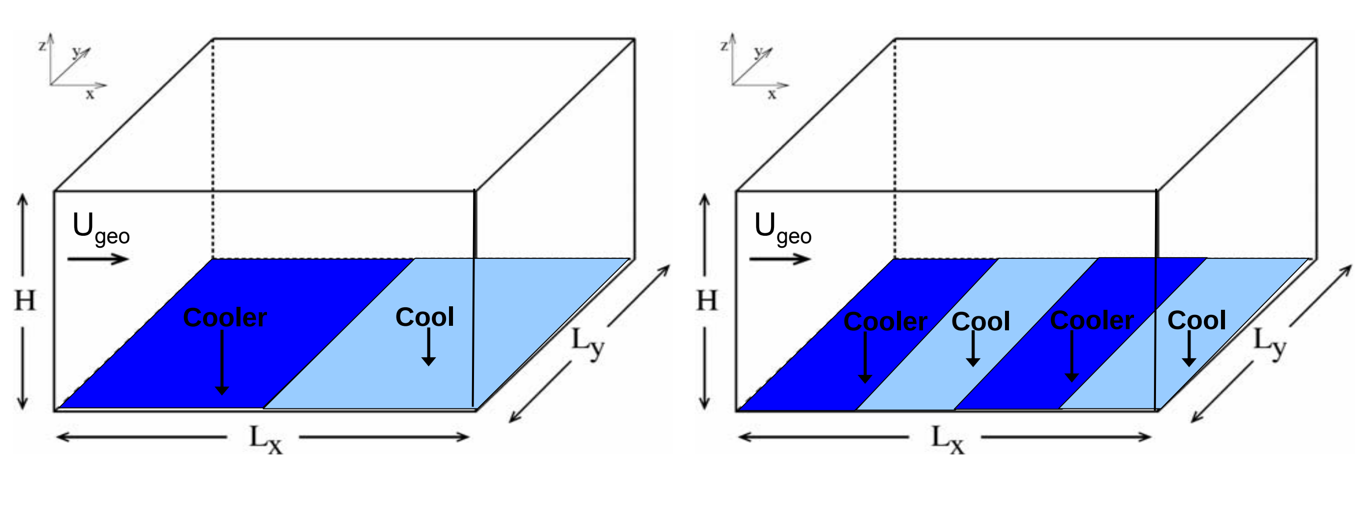

Figure 8: Example schematics of the surface temperature patterns used in the heterogeneous SBL cases for the 400 m (left) and 200 m (right) patch sizes.

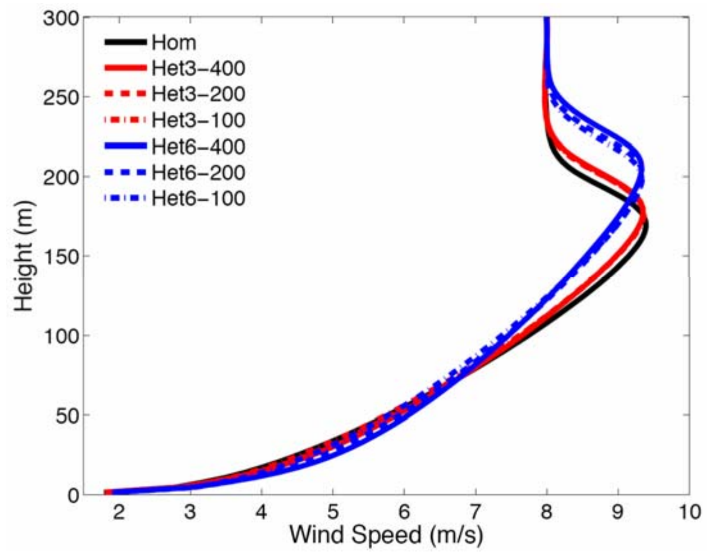

Figure 9: Mean wind speed profile averaged over the last one hour of the simulation for the homogeneous and heterogeneous stable boundary layer simulations. Legend abbreviations are the same as used in Table 2.

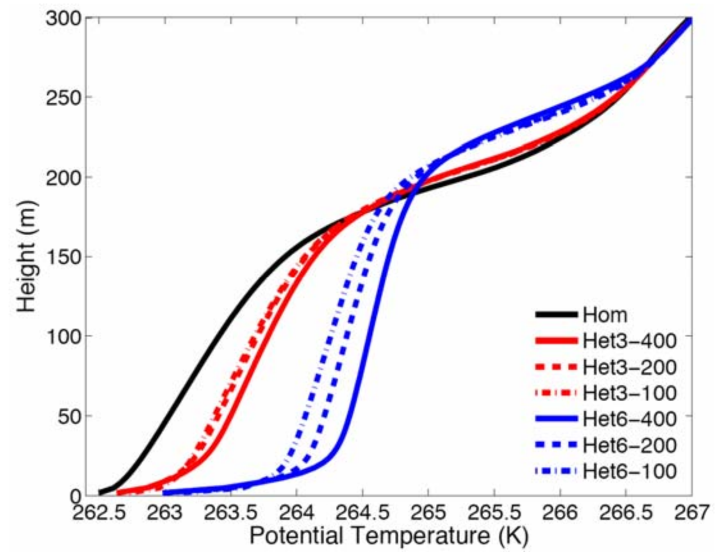

Figure 10: Mean potential temperature averaged over the last one hour of the simulation for the homogeneous and heterogeneous stable boundary layer simulations. Legend abbreviations are the same as used in Table 2.

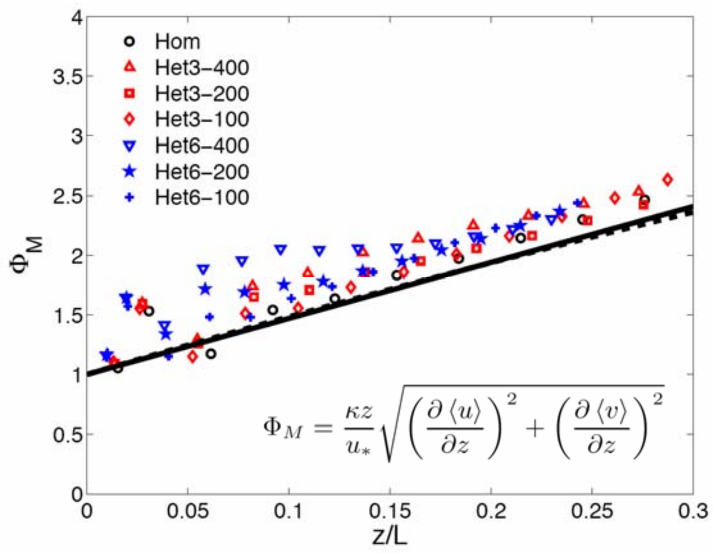

Figure 11: Non-dimensional velocity gradient as a function of z/L in the lowest 50 m of the domain. The solid line and dashed line correspond to the formulations proposed by Businger et al. (1971) and Beljaars and Holtslag (1991), respectively. Legend abbreviations are the same as used in Table 2.

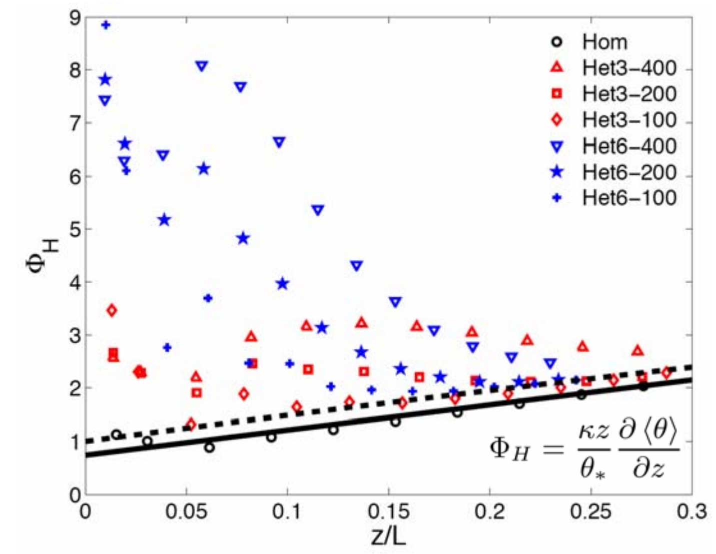

Figure 12: Non-dimensional potential temperature gradient as a function of z/L in the lowest 50 m of the domain. The solid line and the dashed line correspond to the formulations proposed by Businger et al. (1971) and Beljaars and Holtslag (1991), respectively. Legend abbreviations are the same as used in Table 2.

Summary

- LES with the newly developed Scale-dependent Lagrangian dynamic SGS models accurately reproduce basic statistics of homogeneous quasi-steady stable ABLs.
- Surface temperature heterogeneity results in increased potential temperature, Obukhov length and boundary layer height.
- The effect of surface temperature differences is more important than the effect of the size of the heterogeneities for the cases considered.
- Non-dimensional temperature gradients are strongly affected by surface temperature heterogeneity. This limits the applicability of similarity theory to parameterize regional-scale surface fluxes.
- Future research will include quantifying the effect of the degree of organization of remotely sensed surface properties on the boundary layer fluxes using data from the NASA CLPX experiment and the development of new surface layer parameterizations that account for surface heterogeneity in stable boundary layers.

Acknowledgements

The authors gratefully acknowledge funding from NASA (grant NNG06GE256). R.S. is supported by a NASA Earth Systems Sciences fellowship (training grant NNG04GR23H). Computing resources were provided by the University of Minnesota Supercomputing Institute.

References

[1] Basu, S, and Porté-Agel, F. 2006, Large-eddy simulation of stably stratified atmospheric boundary layer turbulence: a scale-dependent dynamic modeling approach. *J. Atmos. Sci.*, in press.

[2] Beare, RJ, MacVean, MK, Holtslag, AAM, Cuxart, J, Esau, I, Golaz, JC, Jimenez, MA, Khairoutdinov, M, Kosovic, B, Lewellen, D, Lund, TS, Lundquist, JK, McCabe, A, Moene, AF, Noh, Y, Raasch, S, and Sullivan, PP. 2006, An intercomparison of large-eddy simulations of the stable boundary layer. *Boundary Layer Meteor.*, DIO 10.1007/s10546-004-2820-6.

[3] Beljaars, ACM, and Holtslag, AAM. 1991, Flux parameterizations over land surfaces for atmospheric models. *J. Appl. Meteorol.*, **30**: 327-341.

[4] Businger, JA, Wyngaard, JC, Izumi, Y, and Bradley, EF. 1971, Flux-profile relationships in the atmospheric surface layer. *J. Atmos. Sci.*, **28**: 181-189.

[5] Meneveau, C, Lund, TS and Cabot, WH. 1996, A Lagrangian dynamic subgrid-scale model of turbulence. *J. Fluid Mech.* **319**: 353-85.

[6] Stoll, R, and Porté-Agel, F. 2006, Dynamic subgrid models for momentum and scalar fluxes in large-eddy simulations of neutrally stratified atmospheric boundary layers over heterogeneous terrain. *Water Resources Res.*, **42(1)**: W01410.